JACS
JOURNAL OF THE AMERICAN CHEMICAL SOCIETY
Article
pubs.acs.org/JACS

Selective NO Trapping in the Pores of Chain-Type Complex Assemblies Based on Electronically Activated Paddlewheel-Type $[Ru_2^{II,II}]/[Rh_2^{II,II}]$ Dimers

Wataru Kosaka,[†] Kayo Yamagishi,[†] Akihiro Hori,[‡] Hiroshi Sato,[§] Ryotaro Matsuda,[§,‡] Susumu Kitagawa,[§,∥,‡] Masaki Takata,[⊥,‡] and Hitoshi Miyasaka*[,#]

[†]Department of Chemistry, Division of Material Sciences, Graduate School of Natural Science and Technology, Kanazawa University, Kakuma-machi, Kanazawa 920-1192 Japan

[‡]RIKEN SPring-8 Center, 1-1-1 Kouto, Sayo-gun, Hyogo 679-5148, Japan

[§]Institute for Integrated Cell-Materials Science (iCeMS), Kyoto University, Katsura, Nishikyo-ku, Kyoto 615-8510, Japan

[∥]Department of Synthetic Chemistry and Biological Chemistry, Graduate School of Engineering, Kyoto University, Katsura, Nishikyo-ku, Kyoto 615-8510, Japan

[⊥]Japan Synchrotron Radiation Research Institute/SPring-8, 1-1-1 Kouto, Sayo-gun, Hyogo 679-5198, Japan

[#]Institute for Materials Research, Tohoku University, 2-1-1 Katahira, Aoba-ku, Sendai 980-8577, Japan

Supporting Information

ABSTRACT: The design of porous materials that undergo selective adsorption of a specific molecule is a critical issue in research on porous coordination polymers or metal−organic frameworks. For the purpose of the selective capture of molecules possessing an electron-acceptor character such as nitric oxide (NO), one-dimensional chain compounds possessing a high donor character have been synthesized using 4-chloroanisate-bridged paddlewheel-type dimetal(II, II) complexes with M = Ru and Rh and phenazine (phz) as the chain linker: $[M_2(4\text{-Cl-2-OMePhCO}_2)_4(phz)]\cdot n(CH_2Cl_2)$ (M = Ru, **1**; Rh, **2**). These compounds are isostructural and are composed of chains with a $[-\{M_2\}-phz-]$ repeating unit and CH_2Cl_2 occupying the void space between the chains. Compounds **1** and **2** change to a new phase (**1-dry** and **2-dry**) upon evacuating the crystallization solvent (CH_2Cl_2) and almost lose their pores in the drying process: no void space in **1-dry** and 31.8 Å^3, corresponding to 2.9% of the cell volume, in **2-dry**. Nevertheless, the compounds show a unique gas accommodation ability. Accompanied by a structural transformation (i.e., the first gate-opening) at low pressures of <10 kPa, both compounds show a typical physisorption isotherm for O_2 (90 K) and CO_2 (195 K), with the adsorption amount of ca. 2−4 gas molecules per $[M_2]$ unit. In addition, the adsorption isotherm for NO (121 K) involves the first gate-opening followed by a second gate-opening anomaly at NO pressures of ≈52 kPa for **1-dry** and ≈21 kPa for **2-dry**. At the first gate-opening, the absorbed amount of NO is ca. 4 molecules per $[M_2]$ unit, and then it reaches 8.4 and 6.3 for **1-dry** and **2-dry**, respectively, at 95 kPa. Only the isotherm for NO exhibits hysteresis in the desorption process, and some of the NO molecules are trapped in pores even after evacuating at 121 K, although it recovers to the original dried sample on heating to room temperature. The adsorbed NO molecules accrue a significant electron donation from the host framework even in the $[Rh_2]$ derivative, indicating that such simple porous compounds with electron-donor characteristics are useful for the selective adsorption of NO.

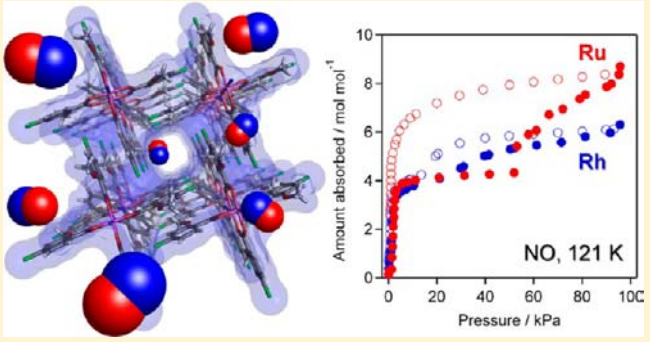

INTRODUCTION

Selective gas adsorption is one of the critical issues in current studies on porous coordination polymer (PCP) and metal−organic framework (MOF) materials.[1,2] In cases where the selectivity of gas adsorption is achieved by tuning the size and shape of pores to the gases to be accommodated, which are found in, for example, conventional materials with homogeneous and robust frameworks such as zeolites and activated carbons, it is not easy to produce specific differences in adsorption properties for different gases.[3] Such robust materials are characterized by invariant characteristics not only for structure but also for electronic properties of frameworks in the adsorption processes, and this point, i.e., "stability" of materials, in fact, has an important consequence for applications of the materials. The most desirable characteristics of PCPs/MOFs

Received: July 24, 2013
Published: October 23, 2013

   dx.doi.org/10.1021/ja4076056 | J. Am. Chem. Soc. 2013, 135, 18469−18480

are their high structural flexibilities and activation capabilities (i.e., functionalization of frameworks). The structural flexibility is a key factor in enhancing selectivity toward specific guest molecules. The corresponding materials undergo a gate open/close, involving expansion/shrinkage of pores, to choose the specific guest molecules.[4] Therefore, as well as recognition by the size and shape of guest molecules, the host−guest interaction is a crucial driving force for the structural transformation, i.e., a key to open the gate. For the purpose of increasing host−guest interactions, therefore, the frameworks are chemically modified with functional groups, and the pores are activated by retaining any reaction site for trapping guest molecules, such as acid−base sites,[2c] chemical-interaction sites,[2d,e,g] redox-active sites,[2f] and so on.[5,6] Among them, the introduction of redox-active sites or chemical-interaction sites into the framework is the most desired function for PCPs/MOFs, which creates not only dynamical but also reactive frameworks completely distinguishable from the nonreactive robust frameworks mentioned above. To date, several intriguing examples have been known, focused on the following subjects: selective recognition through a host−guest charge-transfer interaction,[2f,7] redox catalysis,[7b,e,f] ionic insertion,[7a,d,i] and enhanced charge mobility.[7d,h,i] However, they are still scarce in this active research field.

Recently, our group has demonstrated the utility of carboxylate-bridged paddlewheel-type diruthenium(II, II) complexes ($[Ru_2^{II,II}(RCO_2)_4]$ (RCO_2^- = carboxylate ion) abbreviated hereafter as $[Ru_2^{II,II}]$) as an electron-donor (D) building unit (i.e., reductant) in frameworks made with electron-acceptor (A) building units (so-called D/A-MOFs).[8−15] This is because of the general knowledge that $[Ru_2^{II,II}]$ complexes are relatively easily oxidized to produce one-electron oxidized species $[Ru_2^{II,III}]^+$,[16] but even in covalently bonded frameworks with a [−D−A−] linkage, the charge transfer and electron transfer of DA ↔ $D^{\delta+}A^{\delta-}$ can be tuned in a linear relation between the ionization potential (I_D) of D and the electron affinity (E_A) of A, where A is the family of 7,7,8,8-tetracyanoquinodimethane (TCNQ) and *N*,*N*′-dicyanoquinodiimine (DCNQI) derivatives.[17] Thus, the use of $[Ru_2^{II,II}]$ complexes with high ionization potentials promises the formation of an ionic state or polarized state $D^{\delta+}A^{\delta-}$. Here, we introduce the utility of paddlewheel-type building blocks as redox-active building blocks even against guest molecules in pores, and we report that a quasi-DA chain compound made from a redox-active $[Ru_2^{II,II}]$ complex and a phenazine (phz) linkage selectively absorbs a reaction-active molecule, nitric oxide (NO), compared with other common gases such as O_2, CO_2, and N_2. Furthermore, even in the corresponding $[Rh_2^{II,II}]$ compound, which undergoes a strong charge donation without electron transfer, the specific adsorption of NO is observed, although not higher than that in the $[Ru_2^{II,II}]$ compound. The selective absorption and regulation of the release of NO in materials, desired not only for environmental applications but also for medical/biological applications,[18] are important themes in the science of MOFs/PCPs.[19] These results indicate that PCPs/MOFs with a high redox activity or a high potential for polarizing in their frameworks, but not on redox-active open-metal sites,[19] are also useful for the selective capture of reactive molecules such as NO in pores. This study proposes a simple strategy for the design of PCPs/MOFs for selective gas adsorption.

RESULTS AND DISCUSSION

Design of Redox-Active PCPs Based on Paddlewheel Dimetal Complexes. In D/A-MOFs composed of $[Ru_2^{II,II}]$ complexes and TCNQ/DCNQI derivatives,[8−15] the degree of charge transfer and oxidation state of the frameworks are closely related to the energy gap ($\Delta E_{H-L}(DA)$) between the highest occupied molecular orbital (HOMO) level of $[Ru_2^{II,II}]$ and the lowest unoccupied molecular orbital (LUMO) level of TCNQ/DCNQI, i.e., proportional to the difference between I_D of $[Ru_2^{II,II}]$ and E_A of TCNQ/DCNQI ($h\nu \approx I_D - E_A$),[17] as was well discussed regarding charge-transfer complexes of organic DA combinations.[20,21] The tuning of the HOMO/LUMO levels of D/A building units can be well achieved by modifying substituents on the carboxylate bridge of $[Ru_2^{II,II}]$[22] and TCNQ/DCNQI;[23] for example, putting an electron-releasing substituent on $[Ru_2^{II,II}]$ enhances the electron donation of the $[Ru_2^{II,II}]$ unit (i.e., the HOMO level becomes higher). This idea should also be applicable to the case of host−guest in PCPs/MOFs. Hence, we focused on one-dimensional chain compounds based on $[Ru_2^{II,II}]$ complexes linked by phz to create donor-type PCPs because this type of porous compound, with benzoate-bridged paddlewheel-type $[M_2^{II,II}]$ (M = Cu, Rh) units and pyrazine linkages, is useful for adsorption of several gases.[24] In addition, chain compounds of $[Ru_2^{II,II}]$−phz complexes can be isolated as relatively stable crystals,[25] and some of them provide good porous materials, as demonstrated by CO_2 adsorption.[26] The choice of phz linkage is due to an idea: because N-substituted phz derivatives with electron-releasing substituents such as methyl group (e.g., 5,10-dihydro-5,10-dimethylphenazine) act as good electron donors,[27] the phz moiety capped by donor $[Ru_2^{II,II}]$ units would also have a donor character advantageous for the design of donor-type PCPs.

For the purpose of designing highly redox-active compounds, the family of *o*-anisate-bridged $[Ru_2^{II,II}]$ complexes, $[Ru_2^{II,II}(2\text{-OMe-4-}x\text{-PhCO}_2)_4(THF)_2]$ (x = H, F, Cl), was synthesized and characterized by X-ray crystallography (Supporting Information Tables S1 and S2 and Figure S1), cyclic voltammetry (Supporting Information Table S3, Figure S2), magnetic measurements (Supporting Information Figure S3), and DFT calculations based on their crystal structures (Supporting Information Tables S4−S7, Figures S4−S7; details of these complexes are given in the Supporting Information), where $[Ru_2^{II,II}(2\text{-OMePhCO}_2)_4(THF)_2]$ has already been reported previously (CCDC-846070).[28] Because of the presence of a methoxy group, which is a strong electron-releasing substituent on benzoate, the redox potential ($E_{1/2}([Ru_2^{II,II}]/[Ru_2^{II,III}]^+)$ vs Ag/Ag^+ in THF) found at +60 mV for $[Ru_2^{II,II}(PhCO_2)_4(THF)_2]$ is greatly shifted to a negative region: −228, −178, and −131 mV for x = H, F, and Cl, respectively, in $[Ru_2^{II,II}(2\text{-OMe-4-}x\text{-PhCO}_2)_4(THF)_2]$. The HOMO energy levels estimated by DFT calculations are −3.745, −4.087, and −4.132 eV for x = H, F, and Cl, respectively, in $[Ru_2^{II,II}(2\text{-OMe-4-}x\text{-PhCO}_2)_4(THF)_2]$, which are higher than the −4.133 eV for $[Ru_2^{II,II}(PhCO_2)_4(THF)_2]$. Thus, the family of $[Ru_2^{II,II}(2\text{-OMe-4-}x\text{-PhCO}_2)_4(THF)_2]$ (x = H, F, Cl) is appropriate for donor building units in our concept, and the chain compounds with a phz linkage, together with their $[Rh_2^{II,II}]$ derivatives for comparison (see Supporting Information for $[Rh_2^{II,II}(2\text{-OMe-4-Cl-PhCO}_2)_4(THF)_2]$), have been synthesized: $[M_2^{II,II}(2\text{-OMe-4-}x\text{-PhCO}_2)_4(phz)]\cdot n(CH_2Cl_2)$ (M = Ru, Rh; x = H, F, Cl). Unfortunately, the compounds with x = H are nonporous compounds, and even

dx.doi.org/10.1021/ja4076056 | J. Am. Chem. Soc. 2013, 135, 18469−18480

with x = F, it was difficult to compare between the Ru and Rh compounds because of their different structures. So, here, the compounds with x = Cl (M = Ru, **1**; Rh, **2**) will be discussed.

Crystal Structures of 1 and 2. Compounds **1** and **2**, crystallizing in the triclinic $P\bar{1}$ space group, are isostructural, where a half of the formula unit, with inversion centers at the midpoint of the M−M bond and the center of the phz molecule, was used as an asymmetric unit (Z = 1). ORTEP drawings of the formula units of **1** and **2** with atomic numbering scheme are depicted in Figure 1 (selected bond distances and angles are given in Supporting Information Table S14). The chain feature is similar to that in $[Ru_2^{II,II}(CF_3CO_2)_4(phz)]$[25] and $[Rh_2^{II,II}(C_2H_5CO_2)_4(phz)]$,[29] forming a linear mode with a [−(M_2)−phz−] repeat along the a-axis. The paddlewheel [M_2] unit with metal−metal bonds remains in the chains with the [$M_2^{II,II}$] oxidation state; in particular, the oxidation state of the [Ru_2] unit in **1** can be confirmed by the local dimensions of the structure (see Table S14 and the related description in the Supporting Information). The asymmetric unit contains two crystallographically unique anisate moieties, which are distinguished hereafter as **anis-A** and **anis-B**, located nearly along the c- and b-axes, respectively (see Figures 2 and S10 in the Supporting Information). The position of the anisate group, i.e., rotation (θ) and bend (ϕ) angles versus the carboxylate group (inset figure in Supporting Information Table S14), is closely associated with the packing form and size of the void space. The (θ, ϕ) angles for **anis-A** and **anis-B** are (10.6°, 3.8°) and (13.6°, 3.1°) for **1** and (10.3°, 3.5°) and (14.4°, 3.7°) for **2**, where θ is obtained as the dihedral angle between the least-squares planes on the phenyl ring of the anisate ligand and a carboxylate-bridging mode (the atom set of Ru_2O_2C), and ϕ is obtained as the angle between a carboxylate-bridging plane and C−C bond between the phenyl ring and the carboxyl carbon (inset figure in Supporting Information Table S14).

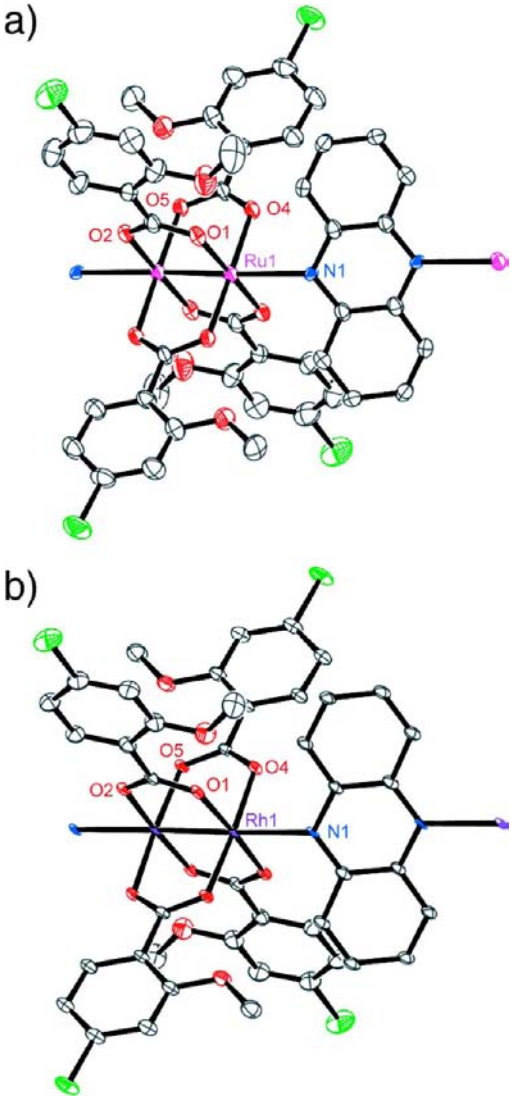

Figure 1. Thermal ellipsoid plots with atom numbering scheme showing the asymmetric unit of **1** (a) and **2** (b) (50% probability ellipsoids), where atoms N, O, C, Cl, Ru, and Rh are represented in blue, red, gray, green, purple, and violet, respectively. Hydrogen atoms and crystal solvents are omitted for clarity.

The chains align in an in-phase manner toward both b- and c-axis directions, and hence, interchain distances, e.g., defined by [M_2]···[M_2], correspond respectively to the lattice constants b and c. Because the θ and ϕ angles are relatively small for the **anis-A** and **anis-B** groups in **1** and **2**, both phenyl planes of **anis-A** and **anis-B** enable the formation of face-to-face π stacks with those of the neighboring chains with distances between π-planes for **anis-A** and **anis-B** of 3.51 and 3.43 Å for **1** and 3.48 and 3.37 Å for **2**. This very orderly alignment of chains allows production of some void spaces along the chain occupied by crystallization solvent CH_2Cl_2 with a solvent-accessible volume of 460.3 Å^3 for **1** and 453.4 Å^3 for **2**, which correspond to 32.3% for **1** and 32.1% for **2** of the total volume (Figures 2 and Supporting Information Figure S10).

Preparation of Dried Compounds and Their Thermal Stability. Compounds **1** and **2** undergo a crystal-to-crystal phase transition upon removal of the crystallization solvents to produce their dried samples, **1-dry** and **2-dry**, respectively. This structural change could be followed by thermal gravimetric analysis (TGA): at an ambient pressure of N_2 atmosphere, **1** and **2** experience a weight loss of 15.1% and 16.0%, respectively, at temperatures reaching ca. 330 K (Figure 3), which corresponds to the release of crystallization solvent (one CH_2Cl_2 per unit). However, the observed values of weight loss are smaller than the calculated values based on their single-crystal structural analyses (calcd: 23.2% and 20.7% for **1** and **2**, respectively), so a part of the crystallization solvent should start to be lost even at room temperature. Compounds **1-dry** and **2-dry** are highly thermally stable, as shown by the fact that the TGA curves show a plateau after releasing CH_2Cl_2 up to ca. 470 K for **1-dry** and 500 K for **2-dry**. The X-ray powder diffraction (XRPD) pattern of **1-dry** drastically changes from that of **1**, but the crystallinity is still maintained, as shown in Figure 4. When **1-dry** is exposed to CH_2Cl_2 vapor for 48 h, the diffraction pattern returns to the original pattern for **1** (Figure 4), indicating a reversible structural variation in the solvation/desolvation process. This variation is basically the same for **2** and **2-dry** (Supporting Information Figure S11). Thus, the samples of **1-dry** and **2-dry** discussed hereafter were prepared by heating at 373 K under vacuum for 5 h.

Crystal Structures of 1-dry and 2-dry. The crystal structures of **1-dry** and **2-dry** were determined on the basis of synchrotron XRPD data using the Rietveld refinement technique (Supporting Information Figure S12). Both compounds crystallize in the triclinic $P\bar{1}$ space group (Z = 1) with an isostructural feature (Supporting Information Table S15).

dx.doi.org/10.1021/ja4076056 | J. Am. Chem. Soc. 2013, 135, 18469−18480

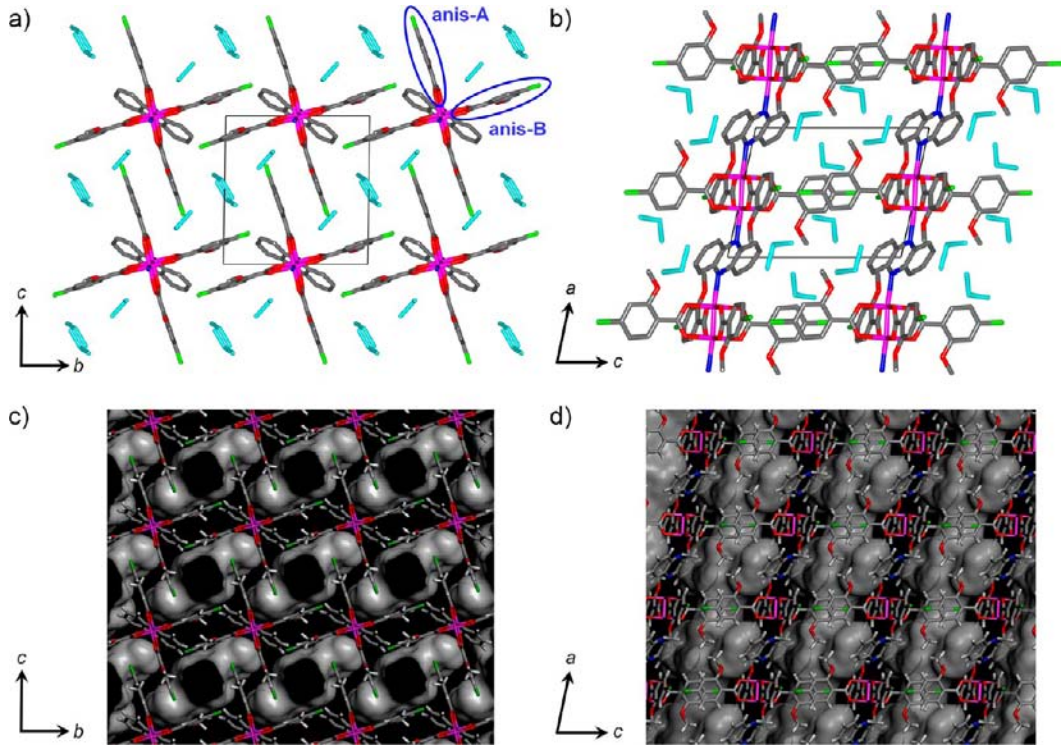

Figure 2. Views of the crystal structure of **1**: the projection in the *bc*-plane (a and c) and the *ac*-plane (b and d), where atoms N, O, C, Cl, and Ru are represented in blue, red, gray, green, and purple, respectively, CH_2Cl_2 molecules as crystallization solvents are given in parts a and b in cyan, and Connolly surface representations of the one-dimensional channels in **1** are displayed in parts c and d. Hydrogen atoms are omitted for clarity.

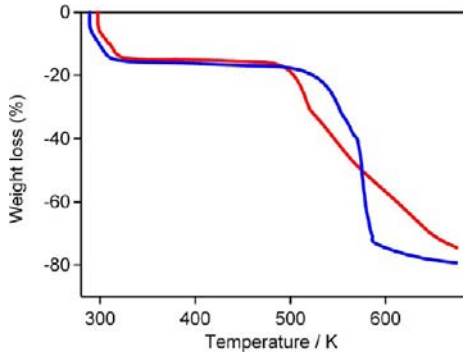

Figure 3. TGA profiles of **1** (red) and **2** (blue) with a heating rate of 5 K min^{-1}.

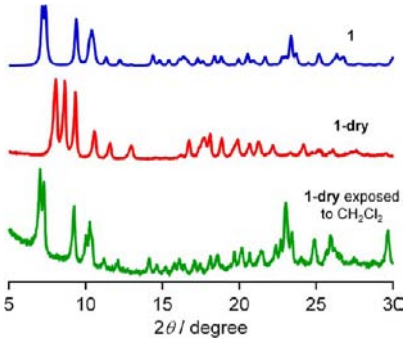

Figure 4. XRPD patterns of **1** simulated from the single-crystal structure (blue), **1-dry** obtained by drying **1** in vacuo at 373 K for 2 h (red), and **1-dry** exposed to CH_2Cl_2 vapor at 298 K for 48 h (green) (Cu Kα radiation with λ = 1.54 Å).

After the removal of crystallization solvent, the unit cell contracts in the *b*- and *c*-axis directions corresponding to the chain-stacking directions, while the *a*-axis lattice constant remains almost unchanged because the *a*-axis is the direction along the chain, resulting in a shrinkage of the unit cell with a volume of 77.3% for **1-dry** and 77.7% for **2-dry** versus the respective volumes of **1** and **2**. Even in **1-dry**, the valence of the $[Ru_2]$ unit is unchanged, which is confirmed by local bond lengths (Supporting Information Table S15) and magnetic properties (Supporting Information Figure S14). The one-dimensional chain motif of **1-dry** and **2-dry** is preserved (Figures 5 and S13 in Supporting Information for **1-dry** and **2-dry**, respectively), but the chain alignment is greatly altered from **1** and **2**; that in the *c*-axis direction is changed from the in-phase manner for the original to an antiphase manner, where the nearest interchain $[M_2]\cdots[M_2]$ and $[M_2]\cdots$phz distances (midpoint-to-midpoint) are both moderate at 10.76 and 10.48 Å for **1-dry**, and 10.64 and 10.39 Å for **2-dry**, which could result from the increase in the angle β. This change in packing results in the disappearance of face-to-face π-stacking in the **anis-A** moieties but leads to a close contact between the chlorine atom of **anis-A** and the π-plane of phz with a distance of 3.15 and 3.14 Å for **1-dry** and **2-dry**, respectively. Meanwhile, the **anis-B** moiety also loses the π-stacking with increasing θ value, 46.8° and 41.6° for **1-dry** and **2-dry**, respectively. The chlorine atom of **anis-B** has short distances of 2.98 and 3.00 Å for **1-dry** and **2-dry**, respectively, with the π-plane of **anis-A** in a neighboring chain. The coordination mode of **anis-B** is instead distorted in **1-dry** and **2-dry** compared with the original modes, which can be explained by the increase in angle ϕ (its definition was given in the previous section) with 18.2° for **1-dry** and 25.7° for **2-dry** (Supporting Information Table S15), although the angle ϕ is, in general, nearly zero in

dx.doi.org/10.1021/ja4076056 | J. Am. Chem. Soc. 2013, 135, 18469−18480

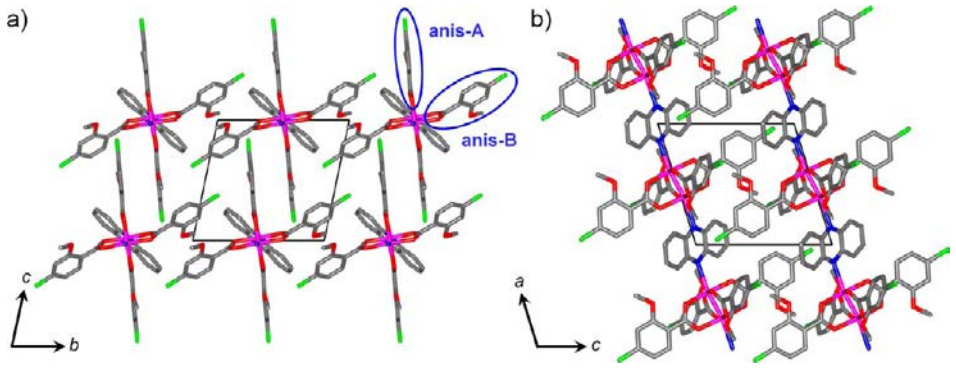

Figure 5. Views of the crystal structure of **1-dry**: the projection in the *bc*-plane (a) and the *ac*-plane (b), where atoms N, O, C, Cl, and Ru are represented in blue, red, gray, green, and purple, respectively. Hydrogen atoms are omitted for clarity.

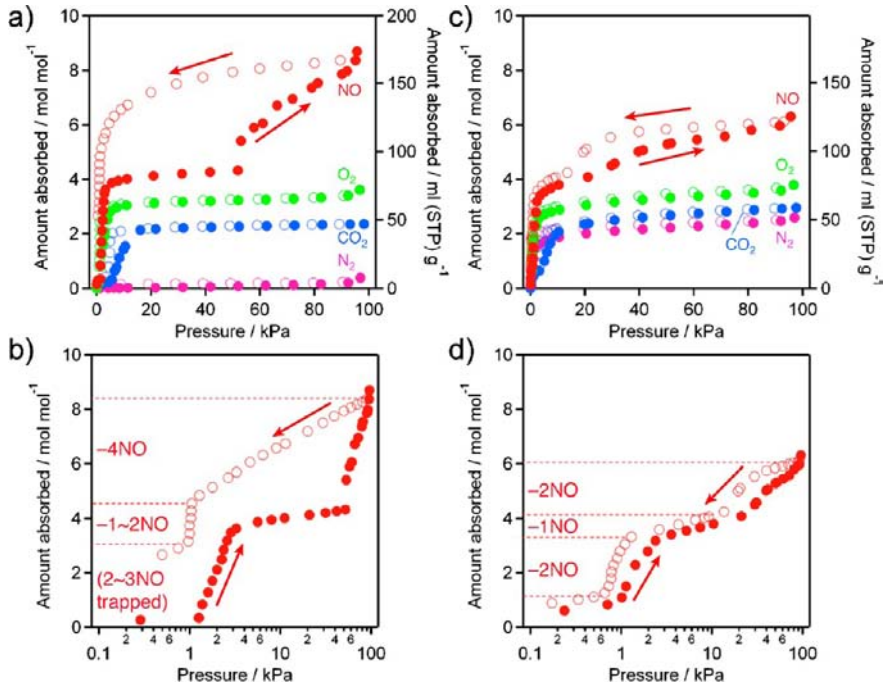

Figure 6. Absorption (closed) and desorption (open) isotherms for several gas molecules, N_2 at 77 K (pink), CO_2 at 195 K (blue), O_2 at 90 K (green), and NO at 121 K (red), for **1-dry** (a, b) and **2-dry** (c, d), where parts b and c are log-scale representations for NO isotherms in **1-dry** and **2-dry**, respectively, and the amount of NO molecules noted indicates the approximate amount of released molecules estimated for each step in the desorption process.

the family of benzoate-bridged paddlewheel-type dinuclear complexes.[16,22] These structural changes involving ≈23% shrinkage in cell volume result in a significant reduction in void space in **1-dry** and **2-dry**: there is no void volume in **1-dry**, and only 31.8 Å^3, corresponding to 2.9% of the cell volume, in **2-dry**.

Sorption Properties. Although there is little void space, **1-dry** and **2-dry** adsorb several gases, because they selectively open a gate dependent on gases accommodated to produce a unique crystal phase of **1-dry⊃G** and **2-dry⊃G** (G: an inserted gas molecule), indicating gas-pressure-dependent structural changes. Figure 6 shows the adsorption isotherms of **1-dry** and **2-dry**. **1-dry** reveals nonporous behavior for N_2 at 77 K, which should be due to the slow diffusion of gaseous molecules into its micropores at such a low temperature as 77 K, as also seen in a similar $[Ru_2^{II,II}]$ chain compound.[26] **2-dry** shows a moderate adsorption of N_2 at 77 K with an adsorbed amount of 54 mL (stp) g^{-1} corresponding to 2.5 molecules per $[Rh_2]$ unit at 90 kPa. This contrasting behavior of **2-dry** compared with **1-dry** indicates that the chains of **2-dry** are more loosely packed than those of **1-dry**, as shown from the difference in their pore volume. For both compounds, the adsorption isotherms of O_2 at 90 K and CO_2 at 195 K show a steep rise at relatively low pressures, indicating a typical physisorption behavior (type I in the International Union of Pure and Applied Chemistry (IUPAC) classification).[30] The adsorbed amounts of O_2 and CO_2 at 90 kPa are 68 and 47 mL (stp) g^{-1} (2.3 and 3.4 molecules per $[Ru_2]$ unit), respectively, for **1-dry**, and 78 and 64 mL (stp) g^{-1} (2.9 and 3.6 molecules per $[Rh_2]$ unit), respectively, for **2-dry**. Thus, the micropores of **1-dry** and **2-dry** have basically the same character for inert gases.

In contrast, the adsorption isotherm of NO shows stepwise behavior. For **1-dry**, the isotherm shows a steep rise because of "the first gate-opening" at low pressures to give a plateau below 52 kPa with an absorbed amount reaching 86 mL (stp) g^{-1} (4.3 molecules per $[Ru_2]$ unit), as is similarly observed in the O_2

dx.doi.org/10.1021/ja4076056 | J. Am. Chem. Soc. 2013, 135, 18469–18480

and CO_2 isotherms, and then, a second abrupt increase begins at 52 kPa, which is "the second gate-opening", to reach an absorbed amount of 167 mL (stp) g^{-1} (8.4 molecules per [Ru_2] unit) at 95 kPa. The adsorption isotherm for **2-dry** also shows stepwise behavior; the plateau region is observed below 21 kPa with an absorbed amount of 89 mL (stp) g^{-1} (4.1 molecules per [Ru_2] unit) followed by the second gate-opening to reach an absorbed amount of 137 mL (stp) g^{-1} (6.3 molecules per [Ru_2] unit) at 96 kPa. A remarkable difference between **1-dry** and **2-dry** is the absorbed amount of NO after the second gate-opening; **1-dry** absorbs ca. two more NO molecules than **2-dry**, although almost the same amount of NO is absorbed in the first step. **2-dry** experiences the second gate-opening at a lower gate-opening pressure than **1-dry**, which should be attributed to the fact that **2-dry** has a looser packing than **1-dry**. In addition to the specific behavior of the NO adsorption isotherm, the desorption isotherm of NO reveals a distinct difference from inert gases: a hysteretic feature is observed (Figure 6). The NO desorption isotherm of **2-dry** almost superimposes on the adsorption isotherm below 10 kPa (Figure 6c,d), whereas the desorption isotherm in **1-dry** never merges into the adsorption isotherm (Figure 6a,b), resulting in a wider hysteresis in **1-dry** than in **2-dry**. The desorption of NO takes place in a stepwise fashion: for **1-dry**, four molecules of NO are gradually released at external pressures down to 1 kPa, leading to a large hysteresis, and 1−2 NO molecules are then released steeply at ca. 1 kPa. Other NO molecules absorbed, 2−3 molecules, are finally trapped at 121 K (Figure 6b) and are released by heating to room temperature (vide infra). Thus, the NO molecule is more strongly trapped in the pores of **1-dry**, even in **2-dry**, and this behavior should be distinguished from the simple physisorption observed for O_2 and CO_2 (note that the adsorption/desorption profiles for O_2 and CO_2 also have small hysteresis features at the first gate-opening process, which are associated with the first-order structural phase transition, but the income/outgo of gases is identical in each gas).

Crystal Structure of 1-dry under Gas Pressure. To confirm the gas-inserted structure, the XRPD for **1-dry** was measured with controlled CO_2 and NO pressures at 195 and 121 K, respectively: the target is **1-dry⊃G** with G = CO_2 and NO (Figure 7). When CO_2 is loaded at less than 1 kPa, the XRPD pattern remains unchanged; however, new peaks appear at 5.2 kPa (Figure 7c), indicating that CO_2 adsorption is going on involving a structural transformation. Above 20 kPa of CO_2 loaded pressure, only the peaks of the new phase for **1-dry⊃CO_2** are observed (Figure 7d,e). The characteristic shift of diffraction peaks in the low-angle region indicates that an expansion of the unit cell occurs in one direction. It should be noted that the original structure is recovered by evacuating CO_2 at 195 K (Figure 7f). A similar structural transformation is observed when NO is loaded as the first step adsorption at 20 kPa, at which the framework structure of **1-dry⊃NO** should be almost the same as that of **1-dry⊃CO_2**, as seen from the peak pattern (Figure 7g). Unfortunately, XRPD measurements for **1-dry⊃NO** at higher NO pressures (i.e., at pressures beyond the second gate-opening pressure) could not be carried out because of a technical problem, as they require a long time to reach NO adsorption equilibrium. Very interestingly, the complete recovery of structure from **1-dry⊃NO** at 20 kPa to the original **1-dry** at 121 K was not successful by only evacuation in vacuo (Figure 7h), despite a vigorous evacuation, but was achieved by evacuating at 200 K (Figure 7i). This aspect indicates that **1-dry** has a characteristic adsorption property for NO, in contrast to physisorption of O_2 and CO_2.

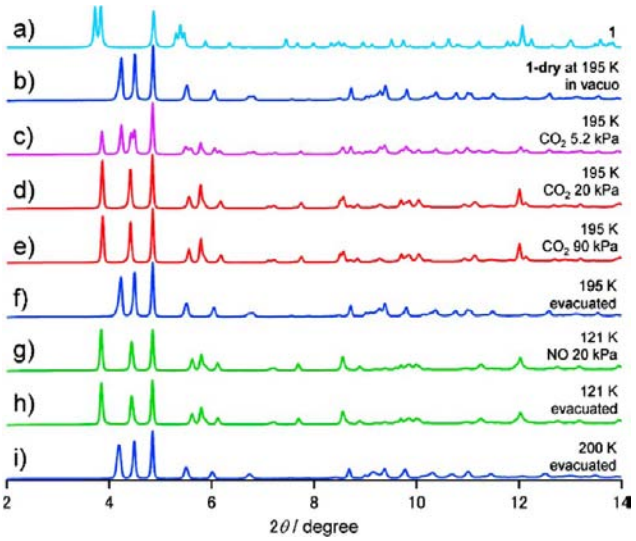

Figure 7. XRPD patterns of **1** and its related samples measured in situ for the gas adsorption/desorption processes: **1** (a), **1-dry** in vacuo at 195 K (b), under 5.2 kPa of CO_2 at 195 K (c), under 20 kPa of CO_2 at 195 K (d), under 90 kPa of CO_2 at 195 K (e), evacuated at 195 K after the CO_2 absorption (f), under 20 kPa of NO at 121 K (g), evacuated at 121 K after the NO absorption (h), evacuated at 200 K after the NO absorption (i) (the wavelength of the incident X-ray is 0.80 Å).

The crystal structures of **1-dry⊃CO_2** and **1-dry⊃NO**, determined by the Rietveld technique (Supporting Information Figure S15), are isostructural ($P\bar{1}$, Z = 1, Supporting Information Table S15), as shown in Supporting Information Figures S16 and 8, respectively. The structural feature of chains is similar to that of **1-dry**, but the unit cell is a little expanded toward the *b*-axis, whereas the *a*- and *c*-axes remain almost unchanged from those of **1-dry**. The chains align in an in-phase manner in the *b*-axis direction; this alignment is unchanged from that in **1-dry**, whereas the chain alignment in the *c*-axis direction is again altered from an antiphase manner in **1-dry** to an in-phase manner seen in the freshly solvated compound **1** (see Supporting Information Table S15 for distances between molecule centers). Neither **anis-A** nor **anis-B** has face-to-face π-stacking, but they show Cl···π-plane contacts in the Cl (**anis-A**)···π-plane (phz) and Cl (**anis-B**)···π-plane (**anis-A**) modes. A marked difference from **1-dry** can be seen in the θ and ϕ values of **anis-B**, which become smaller in **1-dry⊃CO_2** and **1-dry⊃NO** than those for **1-dry** (Supporting Information Table S15), indicating that the strong distortion around **anis-B** observed in **1-dry** was greatly reduced as a result of gas accommodation. Consequently, the one-dimensional channel along the chain axis (i.e., the *a*-axis) is expanded to accommodate two molecules of CO_2 and four molecules of NO per unit (Supporting Information Figures S16 and 8 for **1-dry⊃CO_2** and **1-dry⊃NO**, respectively). Indeed, the pore volume for the accommodation is 159.2 $Å^3$ (13.3%) in **1-dry⊃CO_2** and 173.6 $Å^3$ (14.4%) in **1-dry⊃NO**, expanded from no void space in **1-dry**.

State Observation on the NO Adsorption by in Situ IR Spectroscopy. The adsorption/desorption behavior for NO gas in **1-dry** and **2-dry** differs from that of the physisorption behavior for O_2 and CO_2, as seen in their isotherms in Figure 6. To study the electronic state of absorbed NO molecules, in situ

dx.doi.org/10.1021/ja4076056 | J. Am. Chem. Soc. 2013, 135, 18469−18480

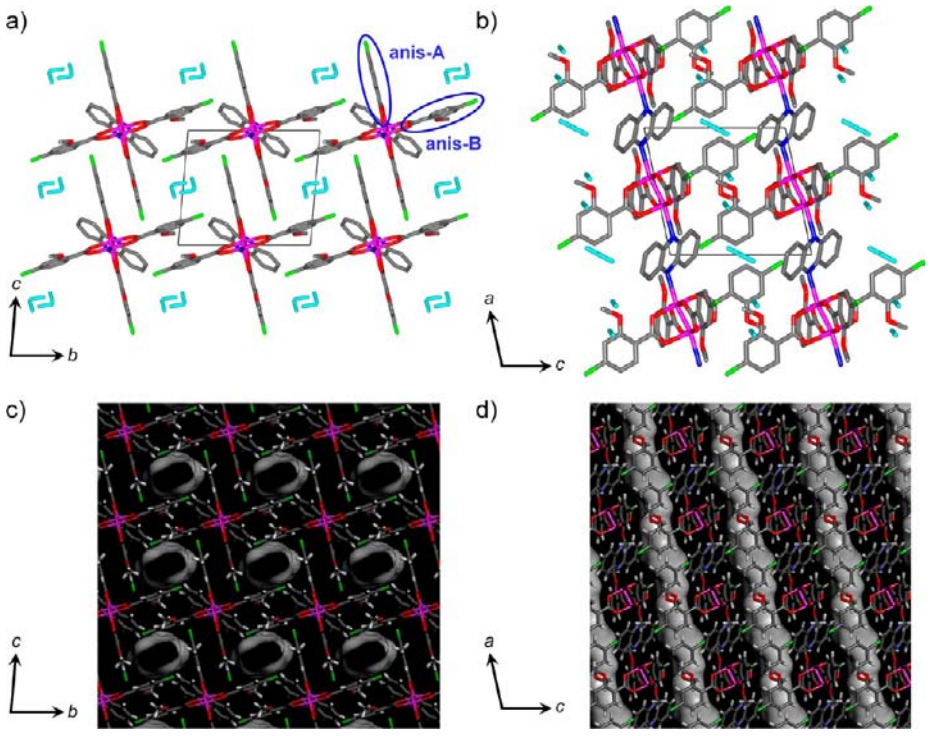

Figure 8. Views of the crystal structure of **1-dry⊃NO**: the projection in the *bc*-plane (a and c) and the *ac*-plane (b and d), where atoms N, O, C, Cl, and Ru are represented in blue, red, gray, green, and purple, respectively, and NO molecules inserted at 121 K are given in parts a and b in cyan, and Connolly surface representations of one-dimensional channels in **1-dry⊃NO** are displayed in parts c and d. Hydrogen atoms are omitted for clarity.

IR spectroscopy at an NO absorption measurement was carried out at 121 K. Various IR spectra measured for several NO absorption/desorption processes are shown in Figure 9, where parts a and b in Figure 9 are in situ IR spectra for the absorption and desorption processes, respectively, and Figure 9c is the NO isotherm measured in situ and represents several pressure points. First, note that the in situ measured isotherm in Figure 9c gives almost the same adsorption profile with stepwise behavior as that measured in the general setup (see Figure 6a).

The vibrational mode of the NO molecule is expected to be observed in the wavenumber range 1600−2000 cm^{-1}, which should shift depending on charge-transfer interactions and charge distributions in the molecule.[31] The observed spectra can be characteristically classified into three regions: band A (1880−1920 cm^{-1}), band B (1720−1880 cm^{-1}), and band C (1660−1720 cm^{-1}). With increasing NO pressure, i.e., in the course of absorption, the intensity of band A monotonically increases. The intensity of band B increases steeply at low pressures <20 kPa, then slowly up to 100 kPa. In contrast, the intensity of band C increases steeply in both the low-pressure (<20 kPa) and high-pressure (>60 kPa) regions. On the other hand, when we see the desorption process (Figure 9b), the intensity of band A decreases monotonically with decreasing NO pressure, but the intensity of band B remains unchanged until the NO pressure becomes less than 20 kPa. Furthermore, the intensity of band C remains unchanged in the whole pressure range, even in vigorous evacuation at 121 K, but recovers to the original by evacuating at room temperature, in agreement with the result of XRPD. For **2-dry**, the variation of IR spectra under NO pressures is basically the same feature as that for **1-dry** (Supporting Information Figure S17).

The variation of peak intensity at 1894, 1847, and 1687 cm^{-1} corresponding to bands A, B, and C, respectively,[31] is plotted as a function of the NO pressure in Figure 10. Judging from the respective energy and NO pressure dependence, band A is assigned as a peak for the stretching mode of gaseous NO (i.e., bulk NO), not for absorbed NO in the framework.[31] The intensities of bands B and C in the low-pressure region <20 kPa are well-synchronized with the abrupt increase of NO absorption, indicating the first gate-opening. However, only band C follows the NO absorption involving the second gate-opening >60 kPa. These results indicate that band B is associated with the absorbed NO gases at the first gate-opening, whereas band C is associated with both the first and second gate-openings. In the desorption process, the intensity of band B suddenly decreases in the low-pressure region (<20 kPa), whereas that of band C remains almost unchanged, indicating that the NO molecules associated with band C have been absorbed more strongly in the framework.

The energies of bands B and C are lower than that of band A for bulk gaseous NO. This means that NO molecules associated with bands B and C are electronically affected in the pores. When the NO molecule acts as an electron acceptor in a charge-transfer set with a donor (i.e., chain frameworks in this work), a charge transfer from the donor should be associated with the antibonding π^* orbital of acceptor NO, which weakens the bond of N−O with a red shift of the stretching IR mode. In addition, it is supposed that the degree of charge transfer δ for $D^{\delta+}\cdots(NO)^{\delta-}$ is larger in band C than in band B; NO molecules of band C are getting a greater electron donation than those of band B. Considering the fact that band C mainly increases in the high NO pressure region >50 kPa, where the second gate-opening occurs, and then remains constant in the desorption process, we realize that charge-transfer interactions between NO molecules and the $[M_2]$−phz framework play an important role in the hysteresis of absorption/desorption processes for NO in **1-dry** and **2-dry**.

dx.doi.org/10.1021/ja4076056 | J. Am. Chem. Soc. 2013, 135, 18469−18480

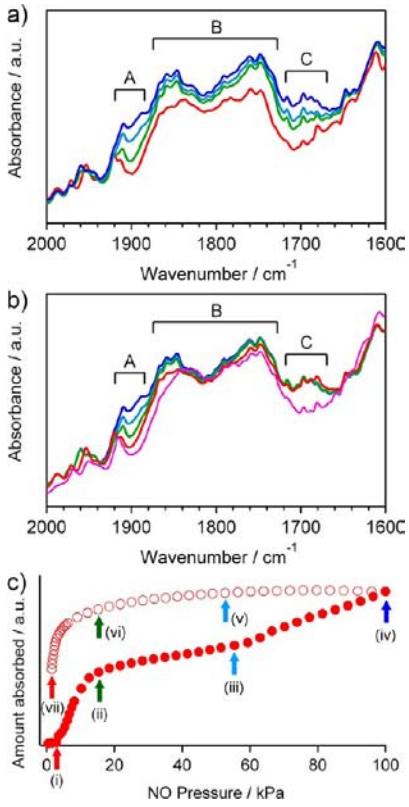

Figure 9. In situ IR spectra measured in the gas adsorption measurements for **1-dry**: (a) IR spectra in the absorption process, where red, green, cyan, and blue spectra were measured at points i, ii, iii, and iv in part c, respectively. (b) IR spectra in the desorption process, where blue, cyan, green, and red spectra were measured at points iv, v, vi, and vii in part c, respectively. The pink spectrum was measured in vacuo at 298 K after the measurement at point vii in part c. (c) Sorption isotherms of NO at 121 K measured using this in situ technique.

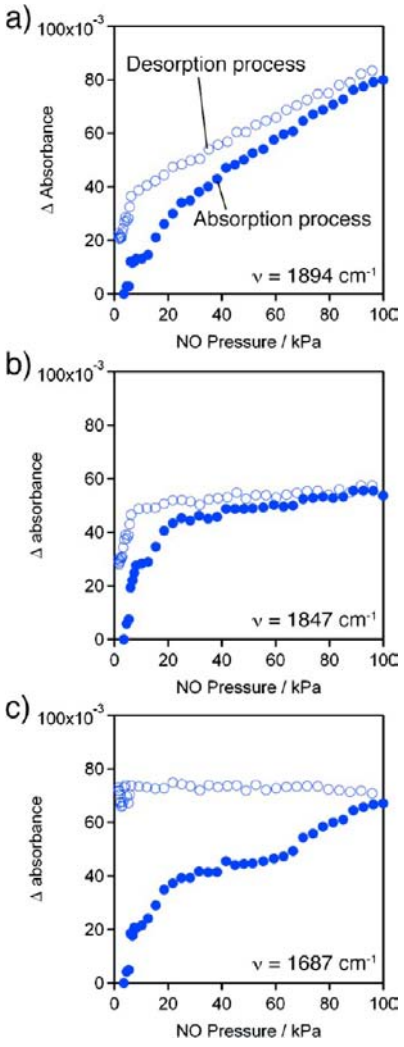

Figure 10. Difference in IR peak intensity for **1-dry** as a function of NO pressure, where the data were taken at 1894 cm^{-1} (a), 1847 cm^{-1} (b), and 1687 cm^{-1} (c), and the closed and open dots are for the absorption and desorption processes, respectively.

Discussion of the Adsorption Properties of This Type of Chain Compound. As shown in the above paragraphs, the chain compounds **1** and **2** experience flexible structural changes as a result of the desolvation involving removal of crystallization solvent (CH_2Cl_2) (**1-dry** and **2-dry**) and the gas adsorptions of CO_2 (**1-dry⊃CO$_2$**) and NO (**1-dry⊃NO**) at 20 kPa, each step of which drastically changes the void volume from 461 $Å^3$ to 0, 159, and 173 $Å^3$ for the series of **1**. Such structural changes are essential for stepwise absorption processes, so a structural change should be involved for the second gate-opening (hereafter referred to as **1-dry⊃NO-h**), although it has not been confirmed experimentally. One of the plausible structures for **1-dry⊃NO-h** is considered to be an analogous structure of **1**, which agrees with the fact that a long time is required to achieve absorption equilibrium at high NO pressures because a drastic structural change should be involved to return to a structure such as **1**. Assuming that the channel shape of **1-dry⊃NO-h** is similar to that of **1**, the main difference in pore shape between **1-dry⊃NO** and **1-dry⊃NO-h** could be found in the adjacent spaces of the π-plane of phz: present for **1** (**1-dry⊃NO-h**), but not for **1-dry⊃NO** (Figures 2, 8, and 11). Hence, it is appropriate to consider that the NO molecules absorbed at high pressures after the second gate-opening fit into pockets around the phz moieties and interact electronically with the phz moiety such as $(phz)^{\delta+}\cdots(NO)^{\delta-}$ (Figure 11). This hypothesis is consistent with the in situ IR data, which show a strong trap for the $(NO)^{\delta-}$ species in the high NO pressure region involving the second gate-opening (vide supra). In addition, the phz moiety N-capped by donor groups or units acts as a good electron donor in which the donating ability is dependent on N-capping donor units. Namely, the charge on phz will be compensated from the $[M_2]$ unit through a metal–ligand charge transfer (MLCT) (Figure 12). As realized from the lower MLCT energy in **1-dry** (Figure 12, Supporting Information Tables S12 and S13), the charge compensation is very effective in **1-dry** because of the higher electron-donating ability of the $[Ru_2]$ unit than $[Rh_2]$ in **2-dry** (energies of the HOMOs calculated for $[Ru_2(4\text{-Cl-2-OMePhCO}_2)_4(phz)_2]$ and $[Rh_2(4\text{-Cl-2-OMePhCO}_2)_4(phz)_2]$ discrete units are −4.3938 and −5.3473 eV, respectively; see Supporting Information Tables S8 and S9). Hence, **1-dry** could absorb a larger amount of NO than **2-dry** after the second gate-opening. Also note that the second gate-opening process observed in the present compounds for NO molecules should be distinguished from that for the specific CO_2 adsorption property in $[Ru_2^{II,II}(p\text{-FPhCO}_2)_4(phz)]$:[26] the former case involves the effect of host–guest interactions, whereas the latter case is basically attributed

dx.doi.org/10.1021/ja4076056 | J. Am. Chem. Soc. 2013, 135, 18469−18480

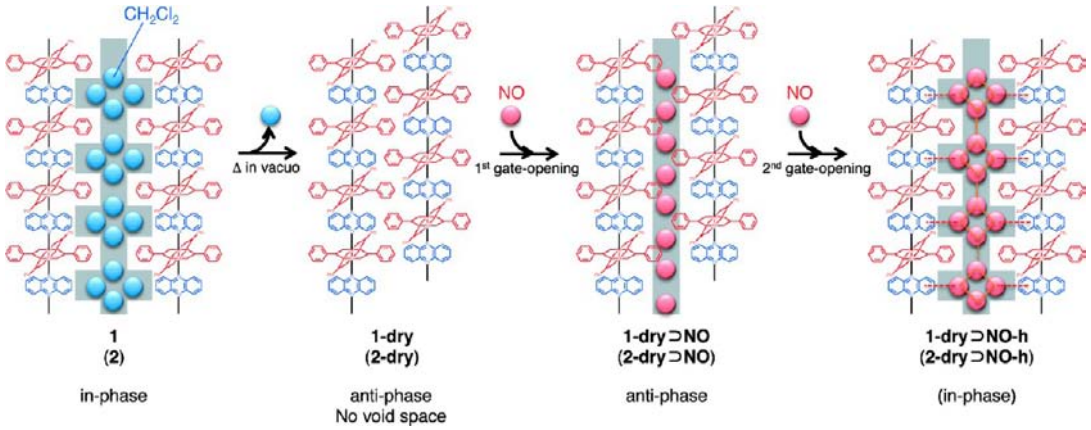

Figure 11. Schematic representations of the variations of structures and void space in the NO-absorption processes from **1** (**2**) to **1-dry⊃NO-h** (**2-dry⊃NO-h**), where the structure of **1-dry⊃NO-h** (**2-dry⊃NO-h**) is a prospective model and the dotted red and orange lines represent interactions. The gray region represents spaces given by the Connolly surface representations in Figures 2 and 8, and the chain arrangement (inphase or antiphase) is noted at the bottom of the models.

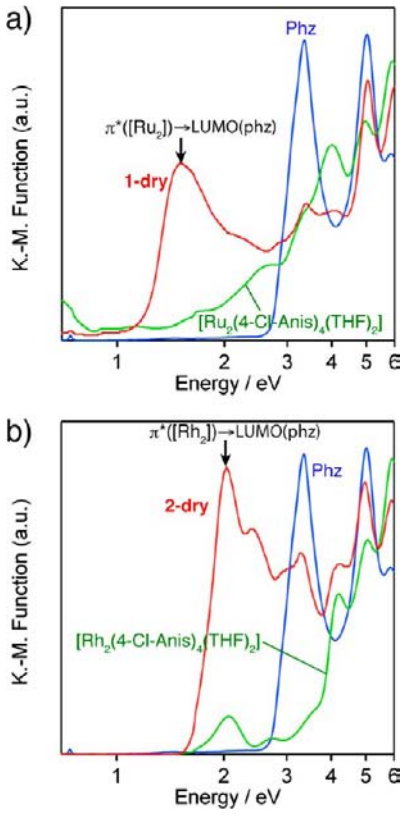

Figure 12. Powder reflectance spectra measured on the basis of $BaSO_4$ pellets: (a) **1-dry** (red), $[Ru_2(4\text{-Cl-2-OMePhCO}_2)_4(THF)_2]$ (green), and phz (blue); (b) **2-dry** (red), $[Rh_2(4\text{-Cl-2-OMePhCO}_2)_4(THF)_2]$ (green), and phz (blue).

to a serendipitous physisorption associated with the nature and size of both pores and guest molecules.

CONCLUSION

In summary, for the purpose of designing PCPs possessing a high electron-donor character, one-dimensional chain compounds composed of paddlewheel-type $[Ru_2]$ and $[Rh_2]$ complexes with 4-chloroanisate as intradimer bridging ligands and phz as chain linkers have been synthesized. This family shows flexible structural transformations triggered by guest molecules; in particular, NO guest molecules induce stepwise transformations with hysteresis absorption/desorption behavior: the first gate-opening absorption step is mainly due to a physisorption by the gas-recognition ability of the pores, as seen in the absorption behavior of CO_2 and O_2, but the second gate-opening absorption step is possibly associated with host/guest chemical interactions, which consequently induce hysteresis in the desorption process. Spectroscopic studies showed that a charge transfer between the host $[-\{M_2\}-phz-]$ framework and NO molecules is present, and this charge-transfer effect plays a key role for the specific adsorption behavior. An important aspect is that the $[M_2]$ unit first incorporated into the system as the main electron donor is indeed not an interactive site in the pores, but the phz unit, which is activated by a π back-donation mechanism from the $[M_2]$ units, and its near-field region are rather important sites, strongly trapping the NO molecules involving charge transfer. From this aspect on the high charge donation of the $[M_2]$ unit, the present strategy used for the design of electronically activated pores would not be achieved as redox-inert $[M_2]$ units such as $[Cu_2]$ are used.[24] Thus, nanosize pores made by PCPs/MOFs possessing a high donor character, even by simple chain compounds of phz-linked $[M_2]$ units, are useful for the chemical capture of NO, and the fine-tuning of electron-donating ability of framework components is a promising strategy to achieve the advanced selective absorption properties.

EXPERIMENTAL SECTION

General Procedures and Materials. All of the synthetic procedures were performed under an inert atmosphere using standard Schlenk-line techniques and a commercial glovebox. All chemicals were purchased from commercial sources and were of reagent-grade quality. Solvents were distilled under a N_2 atmosphere using common drying agents. $[Ru_2(CH_3CO_2)_4Cl]$ and $[Rh_2(CH_3CO_2)_4(MeOH)_2]$ as precursors for $[M_2(4\text{-Cl-2-OMePhCO}_2)_4(THF)_2]$ (M = Ru, Rh) were synthesized by literature methods.[32] Because **1** and **2** easily lose their crystallization solvents even at room temperature (see text), elemental analysis was not carried out for the original **1** and **2** but was performed for **1-dry** and **2-dry**. Fresh samples taken immediately from the mother liquids were used for magnetic measurements, and the formula determined by single-crystal X-ray crystallography was used for the data analyses.

Preparation of $[Ru_2(4\text{-Cl-2-OMePhCO}_2)_4(THF)_2]$. $[Ru_2^{II,III}(CH_3CO_2)_4Cl]$ (1.42 g, 3.0 mmol) and 4-chloro-2-methox-

dx.doi.org/10.1021/ja4076056 | J. Am. Chem. Soc. 2013, 135, 18469−18480

ybenzoic acid (2.24 g, 12.0 mmol) were refluxed in 150 mL of MeOH for 48 h. After cooling to room temperature, Zn powder (392 mg, 6.0 mmol) was added to the solution and then refluxed for 24 h. After removal of the solution by hot filtration, the brown residue was dried in vacuo. The residue was dissolved in 100 mL of THF and refluxed for 24 h. The brown solution was filtered and then layered with *n*-hexane to obtain brown crystals after one week (2.19 g, yield: 67%). Elemental analysis (%) calcd for $C_{40}H_{40}Cl_4O_{14}Ru_2$: C 44.13, H 3.70. Found: C 44.40, H 3.75. IR (KBr): $\nu(CO_2)$, 1544, 1403, 1378 cm^{-1}.

Preparation of 1. A solution of $[Ru_2(4\text{-Cl-2-OMePh-}CO_2)_4(THF)_2]$ (44 mg, 0.04 mmol) in CH_2Cl_2 (10 mL) was separated into five portions and placed in narrow-diameter glass tubes (ϕ 8 mm) (bottom layer). Then, a mixed solvent of CH_2Cl_2/benzene 1:1 v/v (1 mL) was placed on the bottom layer to slow the rate of diffusion (middle layer). Finally, a solution (2 mL) of phz (28 mg, 0.16 mmol) in benzene (10 mL) was carefully placed on the middle layer of each bath (top layer). The glass tubes were left undisturbed for one week to obtain needle-type brown crystals of **1** (yield 63%). IR (KBr): $\nu(CO_2)$, 1539, 1411, 1379 cm^{-1}.

Preparation of 1-dry. Compound **1** was heated to 373 K under vacuum for 5 h. Elemental analysis (%) calcd for $C_{44}H_{32}Cl_4N_2O_{12}Ru_2$: C 46.99, H 2.87, N 2.49. Found: C 46.97, H 2.98, N 2.61. IR (KBr): $\nu(CO_2)$, 1539, 1409, 1377 cm^{-1}.

Preparation of $[Rh_2(4\text{-Cl-2-OMePhCO}_2)_4(THF)_2]$. $[Rh_2(CH_3CO_2)_4(MeOH)_2]$ (506 mg, 1 mmol) and 4-chloro-2-methoxybenzoic acid (1.36 mg, 8.0 mmol) were refluxed in 20 mL of diglyme for 2 h. After removal of the solvent in vacuo, the green residue was washed with *n*-hexane and dissolved in the minimum amount of THF. The green solution was filtered and then layered with *n*-hexane to obtain green crystals after one week (568 mg, yield: 52%). Elemental analysis (%) calcd for $C_{40}H_{40}Cl_4O_{14}Rh_2$: C 43.98, H 3.69. Found: C 43.74, H 3.91. IR (KBr): $\nu(CO_2)$, 1602, 1406, 1377 cm^{-1}.

Preparation of 2. This complex was prepared using a procedure similar to that used for **1** but using $[Rh_2(4\text{-Cl-2-OMePh-}CO_2)_4(THF)_2]$ (44 mg, 0.04 mmol), giving needle-type dark-green crystals of **2** (yield 45%). IR (KBr): $\nu(CO_2)$, 1603, 1408, 1378 cm^{-1}.

Preparation of 2-dry. The dried form was prepared using a procedure similar to that used for **1-dry**. Elemental analysis (%) calcd for $C_{44}H_{32}Cl_4N_2O_{12}Rh_2$: C 46.84, H 2.86, N 2.48. Found: C 46.80, H 2.93, N 2.60. IR (KBr): $\nu(CO_2)$, 1603, 1409, 1378 cm^{-1}.

Physical Measurements. Infrared (IR) spectra were recorded as KBr pellets with a HORIBA FT-720 spectrometer. The thermogravimetric analyses (TGA) were recorded on a Shimadzu DTG-60H apparatus under N_2 atmosphere in the temperature range between 298 and 573 K at a heating rate of 5 K min^{-1}. X-ray powder diffraction (XRPD) spectra were recorded using an Ultima IV diffractometer with Cu Kα radiation (λ = 1.5418 Å) at room temperature. Powder reflection spectra were measured on pellets diluted with $BaSO_4$ using a Shimadzu UV-3150 spectrometer. Magnetic susceptibility measurements were conducted with a Quantum Design SQUID magnetometer MPMS-XL on a polycrystalline sample in the range 1.8−300 K at 1000 Oe. The data were corrected for the diamagnetic contribution of the sample using Pascal's constants.[33]

X-ray Crystallographic Analyses for 1 and 2. Crystal data for **1** were collected at 123 K on a CCD diffractometer (Rigaku Mercury 70) with graphite monochromated Mo Kα radiation (λ = 0.710 70 Å). Crystal data for **2** were collected at 93 K on a CCD diffractometer (Rigaku Saturn 724) with multilayer mirror monochromated Mo Kα radiation (λ = 0.710 75 Å). A single crystal was mounted on a thin Kapton film using Nujol and cooled in a N_2 gas stream. The structures were solved using direct methods (SHELX97[34] and SIR2008[35] for **1** and **2**, respectively), which were expanded using Fourier techniques. The full-matrix least-squares refinement on F^2 was performed on the basis of observed reflections and variable parameters, and the refinement cycle was estimated from unweighted and weighted agreement factors of R1 = $\Sigma||F_o| - |F_c||/\Sigma|F_o|$ ($I > 2.00\sigma(I)$ and all data) and wR2 = $[\Sigma(w(F_o^2 - F_c^2)^2)/\Sigma w(F_o^2)^2]^{1/2}$ (all data). A Sheldrick weighting scheme was used. Neutral atom scattering factors were taken from Cromer and Waber.[36] Anomalous dispersion effects were included in F_c;[37] the values of $\Delta f'$ and $\Delta f''$ were those of Creagh and McAuley.[38] The values for the mass attenuation coefficients are those of Creagh and Hubbell.[39] All calculations were performed using the CrystalStructure crystallographic software package,[40] except for refinement, which was performed using SHELXL-97.[41] These data have been deposited as CIFs at the Cambridge Data Centre as supplementary publication nos. CCDC-951260 and -951255 for **1** and **2**, respectively. Copies of the data can be obtained free of charge on application to CCDC, 12 Union Road, Cambridge CB21EZ, U.K. (fax (+44) 1223-336-033; e-mail deposit@ccdc.cam.ac.uk). Structural diagrams were prepared using VESTA software.[42] The void volumes of the crystal structures were estimated using PLATON.[43]

Crystallographic Data of 1. Formula: $C_{48}H_{40}Cl_{12}N_2O_{12}Ru_2$, M_r = 1464.43, triclinic, $P\bar{1}$ (No. 2), a = 9.697(2) Å, b = 12.025(3) Å, c = 12.608(3) Å, α = 87.81(3)°, β = 77.56(2)°, γ = 83.71(2)°, V = 1426.8(6) Å^3, T = 123(1) K, Z = 1, D_{calc} = 1.704 g cm^{-3}, F_{000} = 730.00, λ = 0.710 70 Å, μ(Mo Kα) = 11.502 cm^{-1}, 13 741 measured reflections, 5005 unique (R_{int} = 0.0767). R1 = 0.0704 ($I > 2\sigma(I)$), R1 = 0.0858 (all data), and wR2 = 0.1829 with GOF = 1.086. CCDC-951260.

Crystallographic Data of 2. Formula: $C_{48}H_{40}Cl_{12}N_2O_{12}Rh_2$, M_r = 1468.10, triclinic, $P\bar{1}$ (No. 2), a = 9.6402(11) Å, b = 12.001(2) Å, c = 12.543(2) Å, α = 88.673(5)°, β = 77.956(4)°, γ = 83.753(5)°, V = 1410.6(3) Å^3, T = 93(1) K, Z = 1, D_{calc} = 1.728 g cm^{-3}, F_{000} = 732.00, λ = 0.710 75 Å, μ(Mo Kα) = 12.115 cm^{-1}, 9743 measured reflections, 4884 unique (R_{int} = 0.1185). R1 = 0.0631 ($I > 2\sigma(I)$), R1 = 0.0700 (all data), and wR2 = 0.1766 with GOF = 1.092. CCDC-951255.

Structural Determination for 1-dry, 1-dry⊃CO_2, 1-dry⊃NO, and 2-dry from XRPD. The ground samples of **1-dry** and **2-dry** were sealed in a silica glass capillary with an inner diameter of 0.4 mm. The XRPD pattern with good counting statistics was measured using the synchrotron radiation XRPD equipment with a large Debye−Scherrer camera and imaging plate as detectors on the BL44B2 beamline[44] at the Super Photon ring-8 Gev (SPring-8, Hyogo, Japan). The XRPD pattern was obtained with a 0.01° step. To obtain in situ XRPD patterns, the gas-handling system, which possesses valves and pressure gauges to dose and remove gas, was connected to the goniometer head using a stainless steel line.

Cell parameters were determined using DIFFRACplus TOPAS v4.2 software. A Le Bail structureless profile fitting algorithm, which affords refined cell parameters and ab initio structure solution from diffraction data using a direct-space method, was performed using FOX software.[45] The structure refinement was performed using the Rietveld method with RIETAN-FP software.[46] The peak shape was modeled using a Split−Pearson VII function. Soft constraints on bond distances, bond angles, and dihedral angles were adopted throughout the refinement. Hydrogen atoms were placed at calculated positions, and their parameters were not refined. The refinement cycle was estimated from agreement factors of $R_{wp} = [\Sigma w[y - f(x)]^2/\Sigma w y^2]^{1/2}$, where y and $f(x)$ represent the observed intensity and the calculated intensity at a diffraction angle of 2θ, respectively, and $R_B = \Sigma||F_o| - |F_c||/\Sigma|F_o|$. These data have been deposited as CIFs at the Cambridge Data Centre as supplementary publication nos. CCDC-951258, 951257, 951259, and 951254 for **1-dry**, **1-dry⊃CO_2**, **1-dry⊃NO**, and **2-dry**, respectively. Copies of the data can be obtained free of charge on application to CCDC, 12 Union Road, Cambridge CB21EZ, U.K. (fax (+44) 1223−336−033; e-mail deposit@ccdc.cam.ac.uk).

Crystallographic Data of 1-dry. Formula: $C_{44}H_{32}Cl_4N_2O_{12}Ru_2$, M_r = 1124.68, triclinic, $P\bar{1}$ (No. 2), a = 9.8692(4) Å, b = 11.0682(3) Å, c = 10.7563(4) Å, α = 79.836(4)°, β = 106.536(5)°, γ = 86.339(5)°, V = 1100.55(8) Å^3, T = 100(1) K, Z = 1, D_{calc} = 1.697 g cm^{-3}, F_{000} = 562.00, λ = 0.799 090(7) Å, $2\theta_{max}$ = 50.00°, $2\theta_{min}$ = 3.00°, step size = 0.01°. R_{wp} = 0.0278, R_B = 0.0412. CCDC-951258.

Crystallographic Data of 1-dry⊃CO_2. Formula: $C_{46}H_{32}Cl_4N_2O_{16}Ru_2$, M_r = 1212.70, triclinic, $P\bar{1}$ (No. 2), a = 9.7304(3) Å, b = 11.9815(3) Å, c = 10.6288(4) Å, α = 85.399(4)°, β = 101.235(6)°, γ = 83.334(4)°, V = 1200.45(7) Å^3, T = 195(1) K, Z = 1, D_{calc} = 1.678 g cm^{-3}, F_{000} = 606.00, λ = 0.799 330(5) Å, $2\theta_{max}$ = 50.00°, $2\theta_{min}$ = 3.00°, step size = 0.01°. R_{wp} = 0.0577, R_B = 0.0162. CCDC-951257.

Crystallographic Data of 1-dry⊃NO. Formula: $C_{44}H_{32}Cl_4N_6O_{16}Ru_2$, M_r = 1244.71, triclinic, $P\bar{1}$ (No. 2), a = 9.7255(3) Å, b = 12.0456(3) Å, c = 10.5596(3) Å, α = 86.501(3)°, β = 101.224(5)°, γ = 83.605(4)°, V = 1201.49(6) Å^3, T = 121(1) K, Z = 1, D_{calc} = 1.720 g cm^{-3}, F_{000} = 622.00, λ = 0.798 730(3) Å, $2\theta_{max}$ = 50.00°, $2\theta_{min}$ = 3.00°, step size = 0.01°. R_{wp} = 0.0412, R_B = 0.0154. CCDC-951259.

Crystallographic Data of 2-dry. Formula: $C_{44}H_{32}Cl_4N_2O_{12}Rh_2$, M_r = 1128.35, triclinic, $P\bar{1}$ (No. 2), a = 9.7930(4) Å, b = 11.753(4) Å, c = 10.6362(5) Å, α = 81.178(5)°, β = 106.289(6)°, γ = 85.825(6)°, V = 1095.82(9) Å^3, T = 100(1) K, Z = 1, D_{calc} = 1.711 g cm^{-3}, F_{000} = 564.00, λ = 0.798 730(3) Å, $2\theta_{max}$ = 50.00°, $2\theta_{min}$ = 3.00°, step size = 0.01°. R_{wp} = 0.0545, R_B = 0.0187. CCDC-951254.

Gas Adsorption Measurement. The sorption isotherm measurements for N_2 (at 77 K), O_2 (at 90 K), NO (at 121 K), CO_2 (at 195 K) gases were carried out using an automatic volumetric adsorption apparatus (BELSORP max; BEL Inc.) connected to a cryostat system. A known weight (ca. 100 mg) of the dried sample was placed into the sample cell and then, prior to measurements, was evacuated again using the degas function of the analyzer for 5 h at 373 K. Then, the change in the pressure was monitored, and the degree of adsorption was determined by the decrease in the pressure at the equilibrium state.

In Situ Gas Adsorption−IR Spectra Measurement. The sorption isotherm measurement for NO gas was carried out at 121 K using an automatic volumetric adsorption apparatus (BELSORP18-Plus; BEL Inc.) connected to a cryostat system. A known weight (ca. 150 mg) of the dried sample was placed on a copper plate and then, prior to measurements, was evacuated again using the degas function of the analyzer for 5 h at 373 K. Then, the change in the pressure was monitored, and the degree of adsorption was determined by the decrease in the pressure at the equilibrium state. In situ IR spectra measurement was conducted through a ZnSe window on the cryostat system with reflection configuration using a JASCO model VIR-200 Fourier transform infrared spectrometer.

■ ASSOCIATED CONTENT

Ⓢ Supporting Information

CIF format X-ray crystallographic data for **1**, **2**, **1-dry**, **2-dry**, **1-dry⊃CO$_2$**, **1-dry⊃NO**, $[Ru_2(2\text{-OMe-4-}x\text{-PhCO}_2)_4(THF)_2]$ (x = F, Cl), and $[Rh_2(4\text{-Cl-2-OMePhCO}_2)_4(THF)_2]$; figures for structures for $[Ru_2(2\text{-OMe-4-}x\text{-PhCO}_2)_4(THF)_2]$ (x = F, Cl), $[Rh_2(4\text{-Cl-2-OMePhCO}_2)_4(THF)_2]$, **2**, **2-dry**, and **1-dry⊃CO$_2$**; and a table summarizing estimated energy levels of MOs and optical transitions for the relevant compounds, XPRD patterns with the results of Rietveld refinement, magnetic properties, IR spectra under NO for **2-dry**. This material is available free of charge via the Internet at http://pubs.acs.org.

■ AUTHOR INFORMATION

Corresponding Author

miyasaka@imr.tohoku.ac.jp

Notes

The authors declare no competing financial interest.

■ ACKNOWLEDGMENTS

This work was supported by a Grant-in-Aid for Scientific Research (No. 24245012, 25620041, 24750057) and on Innovative Areas ("Coordination Programming" Area 2107, No 24108714) from the Ministry of Education, Culture, Sports, Science, and Technology, Japan, The Sumitomo Foundation, The Asahi Glass Foundation, and The CL-IMR Project. The synchrotron radiation experiments were performed at BL44B2 in Spring-8 with approval of RIKEN (Proposal 20120049).

■ REFERENCES

(1) (a) Kitagawa, S.; Kitaura, R.; Noro, S. *Angew. Chem., Int. Ed.* **2004**, *43*, 2334. (b) Yaghi, O. M.; O'Keeffe, M.; Ockwig, N. W.; Chae, H. K.; Eddaoudi, M.; Kim, H. *Nature* **2003**, *423*, 705. (c) Férey, G. *Chem. Soc. Rev.* **2008**, *37*, 191.

(2) (a) Dybtsev, D. N.; Chun, H.; Yoon, S. H.; Kim, D.; Kim, K. *J. Am. Chem. Soc.* **2004**, *126*, 32. (b) Bourrelly, S.; Llewellyn, P. L.; Serre, C.; Millange, F.; Loiseau, T.; Férey, G. *J. Am. Chem. Soc.* **2005**, *127*, 13519. (c) Matsuda, R.; Kitaura, R.; Kitagawa, S.; Kubota, Y.; Belosludov, R. V.; Kobayashi, T. C.; Sakamoto, H.; Chiba, T.; Takata, M.; Kawazoe, Y.; Mita, Y. *Nature* **2005**, *436*, 238. (d) Vaidhyanathan, R.; Iremonger, S. S.; Dawson, K. W.; Shimizu, G. K. H. *Chem. Commun.* **2009**, 5230. (e) Xiao, B.; Byrne, P. J.; Wheatley, P. S.; Wragg, D. S.; Zhao, X.; Fletcher, A. J.; Thomas, K. M.; Peters, L.; Evans, J. S. O.; Warren, J. E.; Zhou, W.; Morris, R. E. *Nat. Chem.* **2009**, *1*, 289. (f) Shimomura, S.; Higuchi, M.; Matsuda, R.; Yoneda, K.; Hijikata, Y.; Kubota, Y.; Mita, Y.; Kim, J.; Takata, M.; Kitagawa, S. *Nat. Chem.* **2010**, *2*, 633. (g) Sato, H.; Matsuda, R.; Sugimoto, K.; Takata, M.; Kitagawa, S. *Nat. Mater.* **2010**, *9*, 661. (h) Southon, P. D.; Price, D. J.; Mckenzie, C. J.; Kepert, C. J. *J. Am. Chem. Soc.* **2011**, *133*, 10885.

(3) (a) Reid, C. R.; Thomas, K. M. *Langmuir* **1999**, *15*, 3206. (b) Bae, Y. S.; Lee, C. H. *Carbon* **2005**, *43*, 95.

(4) Yang, S.; Lin, X.; Lewis, W.; Suyetin, M.; Bichoutskaia, E.; Parker, J. E.; Tang, C. C.; Allan, D. R.; Rizkallah, P. J.; Hubberstey, P.; Champness, N. R.; Thomas, K. M.; Blake, A. J.; Schröder, M. *Nat. Mater.* **2012**, *11*, 710.

(5) Forgan, R. S.; Smaldone, R. A.; Gassensmith, J. J.; Furukawa, H.; Cordes, D. B.; Li, Q.; Wilmer, C. E.; Botros, Y. Y.; Snurr, R. Q.; Slawin, A. M. Z.; Stoddart, J. F. *J. Am. Chem. Soc.* **2012**, *134*, 406.

(6) Park, J.; Yuan, D.; Pham, K. T.; Li, J.-R.; Yakovenko, A.; Zhou, H.-C. *J. Am. Chem. Soc.* **2012**, *134*, 99.

(7) (a) Choi, H. J.; Suh, M. P. *J. Am. Chem. Soc.* **2004**, *126*, 15844. (b) Moon, H. R.; Kim, J. H.; Suh, M. P. *Angew. Chem., Int. Ed.* **2005**, *44*, 1261. (c) Shimomura, S.; Matsuda, R.; Tsujino, T.; Kawamura, T.; Kitagawa, S. *J. Am. Chem. Soc.* **2006**, *128*, 16416. (d) Férey, G.; Millange, F.; Morcrette, M.; Serre, C.; Doublet, M.-L.; Grenèche, J.-M.; Tarascon, J.-M. *Angew. Chem., Int. Ed.* **2007**, *46*, 3259. (e) Cheon, Y. E.; Suh, M. P. *Angew. Chem., Int. Ed.* **2009**, *48*, 2899. (f) Tonigold, M.; Lu, Y.; Bredenkötter, B.; Rieger, B.; Bahnmüller, S.; Hitzbleck, G.; Volkmer, D. *Angew. Chem., Int. Ed.* **2009**, *48*, 7546. (g) Bloch, E. D.; Murray, L. J.; Queen, W. L.; Chavan, S.; Maximoff, S. N.; Bigi, J. P.; Krishna, R.; Peterson, V. K.; Grandjean, F.; Long, G. J.; Smit, B.; Bordiga, S.; Brouwn, C. M.; Long, J. R. *J. Am. Chem. Soc.* **2011**, *133*, 14814. (h) Halls, J. E.; Hernán-Gómez, A.; Burrows, A. D.; Marken, F. *Dalton Trans.* **2012**, *41*, 1475. (i) Horike, S.; Sugimoto, M.; Kongpatpanich, K.; Hijikata, Y.; Inukai, M.; Umeyama, D.; Kitao, S.; Seto, M.; Kitagawa, S. *J. Mater. Chem. A* **2013**, *1*, 3675.

(8) Miyasaka, H.; Campos-Fernández, C. S.; Clérac, R.; Dunbar, K. R. *Angew. Chem., Int. Ed.* **2000**, *39*, 3831.

(9) Miyasaka, H.; Izawa, T.; Takahashi, N.; Yamashita, M.; Dunbar, K. R. *J. Am. Chem. Soc.* **2006**, *128*, 11358.

(10) Motokawa, N.; Oyama, T.; Matsunaga, S.; Miyasaka, H.; Yamashita, M.; Dunbar, K. R. *CrystEngComm* **2009**, *11*, 2121.

(11) Miyasaka, H.; Motokawa, N.; Matsunaga, S.; Yamashita, M.; Sugimoto, K.; Mori, T.; Dunbar, K. R. *J. Am. Chem. Soc.* **2010**, *132*, 1532.

(12) Motokawa, N.; Matsunaga, S.; Takaishi, S.; Miyasaka, H.; Yamashita, M.; Dunbar, K. R. *J. Am. Chem. Soc.* **2010**, *132*, 11943.

(13) (a) Motokawa, N.; Miyasaka, H.; Yamashita, M.; Dunbar, K. R. *Angew. Chem., Int. Ed.* **2008**, *47*, 7760. (b) Motokawa, N.; Miyasaka, H.; Yamashita, M. *Dalton Trans.* **2010**, *39*, 4724.

(14) Miyasaka, H.; Morita, T.; Yamashita, M. *Chem. Commun.* **2011**, *47*, 271.

(15) Miyasaka, H.; Motokawa, N.; Chiyo, T.; Takemura, M.; Yamashita, M.; Sagayama, H.; Arima, T. *J. Am. Chem. Soc.* **2011**, *133*, 5338.

(16) (a) Cotton, F. A.; Walton, R. A. *Multiple Bonds Between Metal Atoms*, 2nd ed.; Oxford University Press: Oxford, U.K., 1993. (b) Cotton; F. A.; Murillo, C. A., Walton, R. A. *Multiple Bonds*

between Metal Atoms, 3rd ed.; Springer-Science and Business Media, Inc.: New York, 2005.
(17) Miyasaka, H. *Acc. Chem. Res.* **2013**, *46*, 248.
(18) Keefer, L. K. *Nat. Mater.* **2003**, *2*, 357.
(19) (a) Xiao, B.; Wheatley, P. S.; Zhao, X.; Fletcher, A. J.; Fox, S.; Rossi, A. G.; Megson, I. L.; Bordiga, S.; Regli, L.; Thomas, K. M.; Morris, R. E. *J. Am. Chem. Soc.* **2007**, *129*, 1203. (b) McKinlay, A. C.; Xiao, B.; Wragg, D. S.; Wheatley, P. S.; Megson, I. L.; Morris, R. E. *J. Am. Chem. Soc.* **2008**, *130*, 10440.
(20) Torrance, J. B.; Vazquez, J. E.; Mayerle, J. J.; Lee, V. Y. *Phys. Rev. Lett.* **1981**, *46*, 253.
(21) Saito, G.; Yoshida, Y. *Bull. Chem. Soc. Jpn.* **2007**, *80*, 1.
(22) Miyasaka, H.; Motokawa, N.; Atsuumi, R.; Kamo, H.; Asai, Y.; Yamashita, M. *Dalton Trans.* **2011**, *40*, 673.
(23) Nakabayashi, K.; Nishio, M.; Kubo, K.; Kosaka, W.; Miyasaka, H. *Dalton Trans.* **2012**, *41*, 6072.
(24) (a) Takamizawa, S.; Nakata, E.; Yokoyama, H.; Mochizuki, K.; Mori, W. *Angew. Chem., Int. Ed.* **2003**, *42*, 4331. (b) Takamizawa, S.; Nakata, E.; Saito, T. *Angew. Chem., Int. Ed.* **2004**, *43*, 1368. (c) Takamizawa, S.; Nakata, E.; Saito, T.; Akatsuka, T. *Inorg. Chem.* **2005**, *44*, 1362. (d) Takamizawa, S.; Saito, T.; Akatsuka, T.; Nakata, E. *Inorg. Chem.* **2005**, *44*, 1421. (e) Takamizawa, S.; Nakata, E.; Akatsuka, T. *Angew. Chem., Int. Ed.* **2006**, *45*, 2216. (f) Takamizawa, S.; Kojima, K.; Akatsuka, T. *Inorg. Chem.* **2006**, *45*, 4580. (g) Takamizawa, S.; Nakata, E.; Akatsuka, T.; Kachi-Terajima, C.; Miyake, R. *J. Am. Chem. Soc.* **2008**, *130*, 17882. (h) Takamizawa, S.; Nakata, E.; Akatsuka, T.; Miyake, R.; Kakizaki, Y.; Takeuchi, H.; Maruta, G.; Takeda, S. *J. Am. Chem. Soc.* **2010**, *132*, 3783.
(25) Miyasaka, H.; Clérac, R.; Campos-Fernández, C. S.; Dunbar, K. R. *J. Chem. Soc., Dalton Trans.* **2001**, 858.
(26) Kosaka, W.; Yamagishi, K.; Yoshida, H.; Matsuda, R.; Kitagawa, S.; Takata, M.; Miyasaka, H. *Chem. Commun.* **2013**, *49*, 1594.
(27) (a) Goldberg, I.; Shmueli, U. *Acta Crystallogr.* **1973**, *B29*, 421. (b) Endres, H.; Keller, H. J.; Moroni, W.; Nöthe, D. *Acta Crystallogr.* **1980**, *B36*, 1435. (c) Soos, Z. G.; Keller, H. J.; Ludolf, K.; Queckbörner, J.; Wehe, D.; Flandrois, S. *J. Chem. Phys.* **1981**, *74*, 5287. (d) Horiuchi, S.; Kumai, R.; Okimoto, Y.; Tokura, Y. *J. Am. Chem. Soc.* **1999**, *121*, 6757.
(28) Itoh, M.; Asai, Y.; Kamo, H.; Miura, A.; Miyasaka, H. *Chem. Lett.* **2012**, *41*, 26.
(29) Cotton, F. A.; Felthouse, T. R. *Inorg. Chem.* **1981**, *20*, 600.
(30) Gregg, S. J.; Sing, K. S. W. *Adsorption, Surface Area, and Porosity*; Academic Press: London, 1984.
(31) Nakamoto, K. *Infrared and Raman Spectra of Inorganic and Coordination Compounds*, 6th ed.; Wiley-Interscience: New York, 2009.
(32) (a) Mitchell, R. W.; Spencer, A.; Wilkinson, G. *J. Chem. Soc., Dalton Trans.* **1973**, 846. (b) Rempel, G. A.; Legzdins, P.; Smith, H.; Wilkinson, G. *Inorg. Synth.* **1972**, *13*, 90.
(33) Boudreaux, E. A.; Mulay, L. N. *Theory and Applications of Molecular Paramagnetism*; John Wiley & Sons: New York, 1976.
(34) Sheldrick, G. M. *Acta Crystallogr., Sect. A* **2008**, *64*, 112.
(35) Burla, M. C.; Caliandro, R.; Camalli, M.; Carrozzini, B.; Cascarano, G. L.; De Caro, L.; Giacovazzo, C.; Polidori, G.; Siliqi, D.; Spagna, R. *J. Appl. Crystallogr.* **2007**, *40*, 609.
(36) Cromer, D. T.; Waber, J. T. *International Tables for Crystallography*; Kynoch Press: Birmingham, U.K., 1974; Vol. *IV*, Table 2.2A.
(37) Ibers, J. A.; Hamilton, W. C. *Acta Crystallogr.* **1964**, *17*, 781.
(38) Creagh, D. C.; McAuley, W. J. *International Tables for Crystallography*; Wilson, A. J. C., Ed.; Kluwer Academic: Boston, MA, 1992; Vol. *C*, Table 4.2.6.8, pp 219−222.
(39) Creagh, D. C.; Hubbell, J. H. *International Tables for Crystallography*; Wilson, A. J. C., Ed.; Kluwer Academic: Boston, MA, 1992; Vol. *C*, Table 4.2.4.3, pp 200−206.
(40) *CrystalStructure 4.0.1: Crystal Structure Analysis Package*; Rigaku Corp.: Tokyo, Japan, 2000−2010.
(41) SHELX97: Sheldrick, G. M. *Acta Crystallogr.* **2008**, *A64*, 112.
(42) Momma, K.; Izumi, F. *J. Appl. Crystallogr.* **2008**, *41*, 653.
(43) Spek, A. L. *Acta Crystallogr., Sect. A* **1990**, *46*, 194.
(44) Kato, K.; Hirose, R.; Takemoto, M.; Ha, S.; Kim, J.; Higuchi, M.; Matsuda, R.; Kitagawa, S.; Takata, K. *AIP Conf. Proc* **2010**, *1234*, 875−878.
(45) Favre-Nicolin, V.; Černý, R. *J. Appl. Crystallogr.* **2002**, *35*, 734.
(46) Izumi, F.; Momma, K. *Solid State Phenom.* **2007**, *130*, 15.